Letter

Coalescence dynamics of prismatic dislocation loops due to vacancy supersaturation

Cameron McElfresh,[1,*] Nicolas Bertin,[2] Sylvie Aubry,[2] and Jaime Marian[1,†]
[1]*Department of Materials Science and Engineering, University of California, Los Angeles, California 90095, USA*
[2]*Materials Science Division, Lawrence Livermore National Laboratory, Livermore, California 94551, USA*

(Received 22 December 2021; accepted 3 August 2022; published 5 October 2022)

Recovery processes in metals with a high defect concentration are at the heart of a structural alloy's usability in engineering applications. However, such processes take place via nonconservative mechanisms mediated by point defect diffusion and are governed by their interactions with the underlying microstructure. Indeed, one of the main challenges in studying recovery processes is their intrinsic multiscale complexity, which often negates the direct use of experimental techniques. In this Research Letter, we study the mechanism of dislocation loop coalescence in metals by simulating the interaction dynamics between vacancies and prismatic loops using a stochastic framework that seamlessly bridges point defect kinetics with dislocation mechanics. Our simulations reveal two fundamental discoveries: first, that climb processes are governed by local fluctuations that are not captured by continuum elastodiffusion models, and, second, that prismatic loops create internal traps for vacancies, leading to the formation of rings around the perimeter of the loops that affect how coalescence takes place. Our results show an excellent agreement with *in situ* experimental observations of loop coalescence in Fe under irradiation.

DOI: 10.1103/PhysRevMaterials.6.L100601

Background. In materials under far-from-equilibrium situations, such as energetic particle irradiation or rapid quenching from high-temperature conditions, high concentrations of metastable defect structures that are ordinarily very difficult to observe can form. Well-known examples of this are the observation of stacking fault tetrahedra in Au, Al, or Ni [1–4], prismatic dislocation loops in Al, Mo, and Nb [5–12], and the formation of "rafts" of dislocation loops in irradiated Fe and W [13–16]. As well, during cold-working of engineering alloys, large numbers of dislocations are produced, creating metastable conditions that result in high strength and low ductility [17–19]. Annealing and/or thermal aging of these microstructures leads to *recovery*, i.e., evolution of the microstructure towards stable arrangements of defects and dislocations. Such stabilization generally results in an improved toughness and increased thermal resistance [20–22]. For materials with a high concentration of metastable loops, recovery works in the direction of reducing the overall dislocation line length by loop coalescence, both in the case of self-interstitial prismatic loops during irradiation [23,24] and for vacancy-type prismatic loops during annealing of quenched metals [6,25].

Recovery is almost always controlled by nonconservative dislocation processes mediated by point defect motion. As such, it is a time-dependent phenomenon that displays a strong temperature dependence. In the most general case, *coalescence* [26–30], is brought about by point-defect-induced dislocation segment climb, ultimately resulting in a reduction of the total dislocation density in the material. Climb allows dislocations to leave their glide planes, thereby opening up additional plastic relaxation pathways for the defect structures. The resulting *elastodiffusion* problem is solved by coupling vacancy diffusion to the stress fields engendered by the dislocation microstructure, which in turn evolves in response to local defect absorption or emission processes. In fact, therein lies one of the main challenges of modeling recovery processes, as dislocation-defect coevolution comprises a wide range of vastly different length and time scales that must be somehow bridged. A common work-around to close this multiscale gap is to adopt a mean-field description of the point defect subpopulation, considering smoothly varying defect densities and condensing their behavior into effective continuum kinetic laws. Even then, such models have only recently begun to be developed [31–35].

There are numerous situations in physics, however, (i) where the inherent discrete nature of point defects cannot be ignored and (ii) where defects' densities are spatially heterogeneous. In both instances, mean-field solutions are invalidated by their inability to capture spatial and thermal fluctuations. Such is the case in the abovementioned examples of irradiation, where defects are introduced in space-localized bursts, or quenching, when loops are formed through a standard nucleation and growth process governed by fluctuations.

In this Research Letter we study the phenomenon of loop coalescence in bcc metals containing a high number density of prismatic loops. Without loss of generality, we focus on quenched Mo as a representative example of a material containing a high number density of prismatic loops of vacancy character, and later turn our attention to Fe for validation with irradiation experiments. However, note that given the qualitative similarities between vacancy and self-interstitial loops, our approach is general and can capture the coalescence kinetics of both types, depending on the case. As such, the kinetics

*cameron.mcelfresh@gmail.com
†Also at Department of Aerospace and Mechanical Engineering, University of California, Los Angeles, California 90095, USA.

for one type can be qualitatively equated to the kinetics of the other by using the appropriate signs for the relevant material parameters and deformation fields. We employ a recently developed stochastic simulator that captures both vacancy diffusion on atomic scales and dislocation dynamics governed by elasticity within a common numerical framework. As will be shown, this seamless coupling of the atomistic and elastic spatiotemporal scales reveals two striking findings about the loop coalescence process and its connection to materials recovery. Furthermore, our simulations are found to be in excellent agreement with experimental observations of loop coalescence processes.

Theory and models. The basis for the method developed here is the model for dislocation climb proposed by McElfresh *et al.* [36], which self-consistently couples vacancy transport with dislocation dynamics (DD) in a stochastic numerical framework, which we briefly describe next. Vacancy transport is modeled as a standard diffusion or advection process:

$$\frac{\partial C}{\partial t} = D_v \nabla^2 C - \boldsymbol{u} \cdot \nabla C, \tag{1}$$

where D_v is the vacancy diffusivity, C is the vacancy concentration at position $\boldsymbol{x}$ and time t, $\boldsymbol{u}$ is the drift velocity vector, and ∇^2 is the Laplacian. The general solution to the above expression in three dimensions (3D) can be shown to be

$$C(\boldsymbol{x}, t) = (6\pi D_v t)^{-\frac{1}{2}} \exp\left\{-\frac{(\boldsymbol{x} - \boldsymbol{u}t)^2}{4D_v t}\right\}, \tag{2}$$

which can be superposed for all vacancies to give the "wave function" (spatial probability distribution function) for the vacancies in the system. We have derived an expression for the drift velocity of a point particle introducing hydrostatic lattice distortions:

$$\boldsymbol{u} = \frac{D_v}{kT}\frac{\Omega_{\text{rel}}}{3}\nabla \text{Tr}[\boldsymbol{\sigma}(\boldsymbol{x})], \tag{3}$$

where Ω_{rel} is the vacancy relaxation volume and $\text{Tr}[\boldsymbol{\sigma}(\boldsymbol{x})] = \sigma_{kk}(\boldsymbol{x})$ is the hydrostatic stress at each specific vacancy position $\boldsymbol{x}$. Thus, when embedded in an elastic medium containing dislocations, the stress tensor $\boldsymbol{\sigma}(\boldsymbol{x})$ provides the local driving force in the form of a diffusion drift that depends on the gradient of its hydrostatic components. It is important to note that Eq. (2) is strictly valid only when $\boldsymbol{u}$ is independent of the vacancy location, which is not the case here. However, as we demonstrate in the Supplemental Material [37], the exact solution of Eq. (1) (i.e., with spatially dependent $\boldsymbol{u}$) can be satisfactorily approximated by Eq. (2) within the timescales of vacancy diffusion, thus justifying its use throughout the rest of this Research Letter.

We implement a method of sampling jump distances that is consistent with each vacancy's local gradient and satisfies a shifted Gaussian as required by a biased random walk. Complete details of the method and implementation are provided in Refs. [36,38]. The evolution of the vacancy subsystem is then simulated by a kinetic Monte Carlo (kMC) algorithm that accounts for elastic drift effects on vacancy diffusion. In this way the vacancy transport module is self-consistently linked to the DD module. The dislocation dynamics module provides a the stress field at time t everywhere in space and updates the dislocation microstructure on the basis of the number and location of vacancy absorptions or emissions by dislocation segments.

The rates of absorption or emission of vacancies are calculated in a cylindrical volume around a dislocation segment i of size $V_i = \pi b_i^2 l_i$, where $b_i = \|\boldsymbol{b}_i\|$ and l_i are the modulus of the Burgers vector $\boldsymbol{b}_i$ and the segment length, respectively. The integer-valued expression for the local rate of emission of vacancies can then be adapted from the standard expression given by Friedel and Yoshida [39] as

$$\dot{N}_i = \dot{N}_i^0\left[1 - \frac{N_i}{\rho_a V_i}\exp\left(\frac{H_f}{kT}\right)\right], \tag{4}$$

$$\dot{N}_i^0 = \left[\frac{2\pi l_i}{b_i}\left(1 - \frac{\boldsymbol{t}_i \cdot \boldsymbol{b}_i}{b_i}\right)\right]\nu(T), \tag{5}$$

where N_i is the number of vacancies emitted, ρ_a is the atomic density, H_f is the vacancy formation enthalpy, $\boldsymbol{t}_i$ is the segment's unit line tangent, and $\nu(T)$ is a temperature-dependent vacancy jump rate. During a kMC iteration, each dislocation segment has a unique emission rate that is added to the list of event rates to sample in each kMC iteration.

Absorption (emission) of vacancies by a dislocation segment i results in climb along its normal direction by an amount

$$h_i = \pm\frac{N_i \Omega_a b_i}{l_i |\boldsymbol{t}_i \times \boldsymbol{b}_i|^2}, \tag{6}$$

where Ω_a is the atomic volume. h_i is positive (negative) if vacancies are absorbed (emitted).

We define the vacancy diffusivity as $D_v = z f b^2 \nu(T)$, where $z = 8$ is the coordination number of the bcc lattice, $f \approx 0.8$ is a correlation factor, and $b \equiv \|\boldsymbol{b}_i\|$ is the jump distance, which is identical to the Burgers vector modulus. For its part, $\nu(T) = \nu_0 \exp[-E_m(\boldsymbol{x})/kT]$, where ν_0 is the attempt frequency, k is Boltzmann's constant, and T is the absolute temperature. The migration barrier of the vacancy is sensitive to elastic stresses as $E_m(\boldsymbol{x}) = E_m^0 - \boldsymbol{\sigma}(\boldsymbol{x}) : \boldsymbol{\Omega}_{\text{act}}$, where $\boldsymbol{\sigma}(\boldsymbol{x})$ is the stress tensor at the vacancy spatial point $\boldsymbol{x}$, E_m^0 is the defect migration energy in an isotropic medium, and $\boldsymbol{\Omega}_{\text{act}}$ is the activation volume tensor [36]. Vacancy migration at or near dislocation cores (e.g., during pipe diffusion) is by definition inelastic and necessitates an atomistic treatment [40–42], currently beyond the scope of this Research Letter. In the following examples, we simulate Mo single crystals defined by the material parameters listed in Table I. To avoid numerical incompatibilities associated with merging deterministic (DD) and stochastic (kMC) integration algorithms, we cast the entire elastoplastic-diffusive problem within a single stochastic framework, taking advantage of a parallel kMC algorithm to evolve the system as a single-event-driven process. The coupled model has been implemented into the massively parallel PARADIS code [45–47] using a synchronous parallel kMC algorithm [48,49].

Results: Vacancy ring formation. Our first finding of significance is that vacancies flowing into a hexagonal prismatic loop [50] do not get immediately absorbed but instead become trapped at an offset distance from the dislocation segments. This is illustrated in Fig. 1, which shows three instantaneous

TABLE I. Material parameters for Mo used in the present simulations [43,44].

Parameter	Symbol	Units	Value
Lattice parameter	a_0	nm	0.317
Atomic density	ρ_a	m^{-3}	6.45×10^{28}
Atomic volume	Ω_a	b^3	0.77
Relaxation volume	Ω_{rel}	Ω_a	−0.37
Vacancy formation energy	H_f	eV	3.0
Vacancy migration energy	E_m^0	eV	1.6
Attempt frequency	ν_0	Hz	10^{12}
Burgers vector	b	nm	0.27

time snapshots (at $t = 0$, 40, and 80 ms) of the interaction between vacancies and a 40b hexagonal dislocation loop at 1400 K in thermal conditions (no vacancy supersaturation). As the figure shows, vacancies are seen to form a ring outside the loop's perimeter, eventually clustering along the edges of the hexagon. Indeed, inspection of the radial stress field of the loop reveals the existence of a barrier against point defect absorption at an offset distance from the loop segments. This barrier is an intrinsic feature of the stress field of an isolated prismatic loop and is shown in Fig. 2 by a solid black curve. The near-core local hydrostatic stress minima exist as a result of the use of the nonsingular elasticity theory in the DD implementation employed here [51]. More details on this implementation can be found in Refs. [51–53]. It is important to note that this type of structure is not fully relaxed because our method does not capture inelastic effects such as vacancy clustering and/or interactions with dislocation cores that might disrupt it and take it towards more stable configurations. Thus it is more appropriate to refer to these trapped clusters as being in a transient configuration that may not be representative of the ground state of the loops.

Additionally, we have discovered that, rather than approaching the loop from outside the glide cylinder [54], vacancies are funneled through the inner boundaries of the compressive stress cone created by the loop, thereby avoiding encountering the barrier altogether. This is shown in Fig. 3, which includes three snapshots of the spatial distribution of thermal vacancies around a stationary 40b-diameter loop at 1400 K, where the color map indicates the value of Tr($\boldsymbol{\sigma}$) in gigapascals. In this fashion, vacancies can become trapped without having to overcome the stress barrier for the

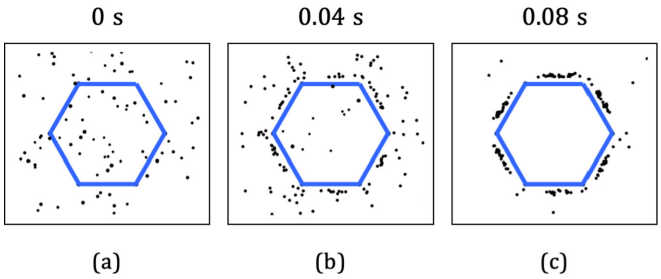

FIG. 1. (a)–(c) Snapshots of vacancy clusters forming around an immobilized vacancy prismatic loop with a core width of 4b. The simulation was performed with a 40b loop at 1400 K.

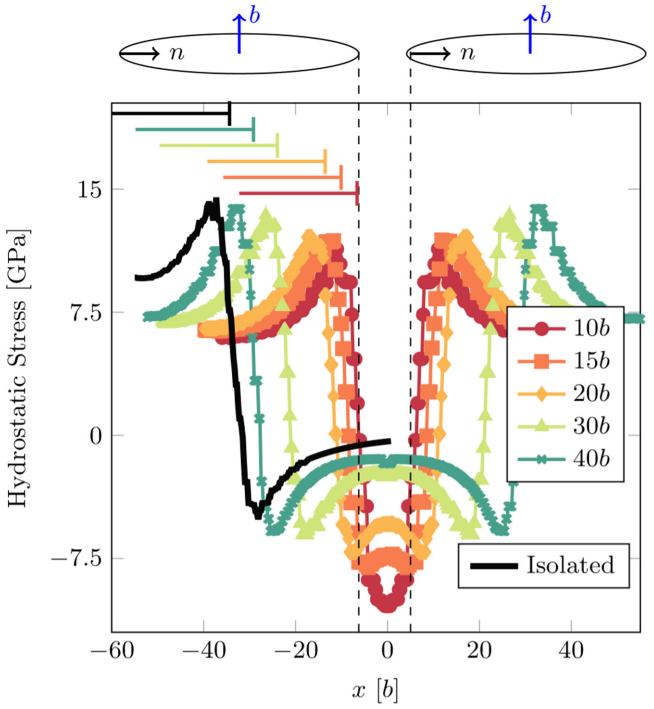

FIG. 2. Hydrostatic stress as a function of the x coordinate between two 40b-diameter vacancy loops at various loop separations. The $x = 0$ value corresponds to the midpoint between the loops' closest points. The two loops drawn above the figure correspond to a separation of 10b. Also shown overlaid in black is the hydrostatic stress profile of an isolated loop.

isolated loop shown in Fig. 2. Indeed, vacancies are accelerated into the loop's perimeter due to the extremely high pressure gradient indicated in the figure. Climb is thus made feasible only after vacancies are able to escape this trap, which is itself a thermally activated process. For completeness, similar evidence of vacancy clustering behavior on the inside of interstitial prismatic loops is provided in the Supplemental Material figures [37].

Results: Loop coalescence mechanism. The stress profile shown in Fig. 2 substantiates the behavior observed in Fig. 1, i.e., that vacancies can arrange themselves into

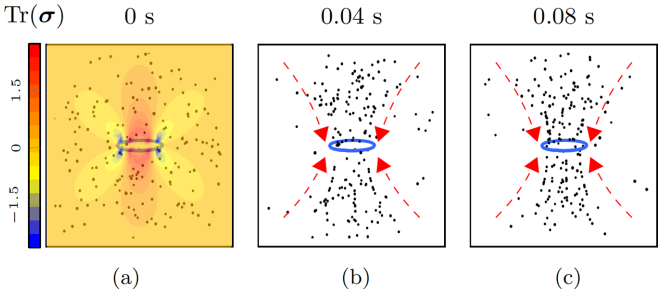

FIG. 3. Kinetic evolution of the vacancies around a 40b-diameter loop at 1400 K. The initial vacancy distribution is shown in (a). The color bar indicates the value of Tr($\boldsymbol{\sigma}$) in gigapascals. The vacancies approach the loop in the fashion indicated by the red arrows in (b) and (c), i.e., following the inner boundaries of the compressive stress lobes created by the loop.

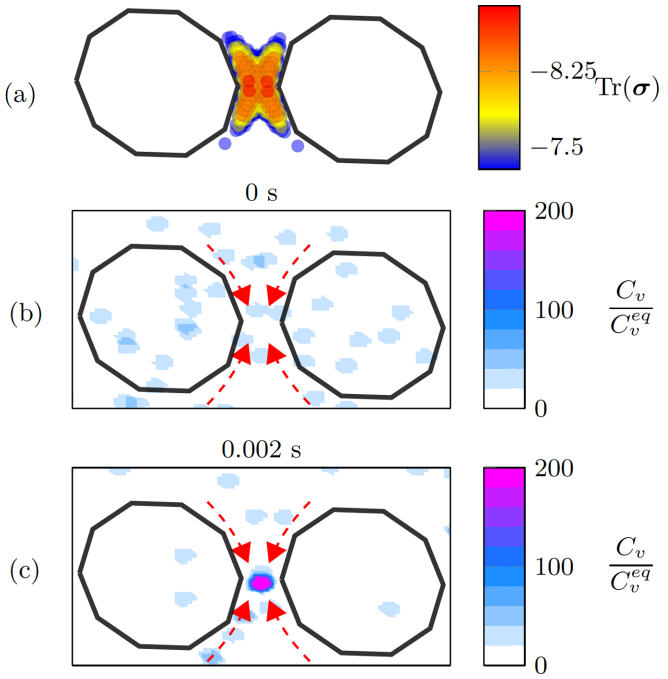

FIG. 4. (a) Hydrostatic stress map for two 60b-diameter vacancy loops separated by 10b. The color bar indicates the value of Tr($\boldsymbol{\sigma}$) in gigapascals. (b) and (c) Local vacancy concentration at $t = 0$ (b) and 0.002 s (c). Red dashed arrows mark the vacancy approach path to the pressure trap shared between the loops.

a ring outside an isolated loop's perimeter. As mentioned earlier, this actually hinders climb, as vacancies are thermodynamically trapped at an offset distance from the actual loop segments. However, when two prismatic dislocation loops approach one another, whether by climb or glide, the situation drastically changes. As Fig. 2 illustrates for a pair of 40b-diameter circular loops, the two stress minima corresponding to the two isolated defects gradually merge with one another, giving rise to a single combined pressure minimum. Most importantly, however, this joint minimum results in an abundance of vacancies trapped in the gap between the loops. Figure 2 shows the shape of the pressure profile at various distances between the two defects. As the loops approach, the shared stress minimum deepens as it is sandwiched between the opposing segments. The stress gradient associated with such a process is seen to increase as well, leading to a strong driving force for vacancy agglomeration in that region, as illustrated in Fig. 4. Furthermore, we have seen that an enhanced accumulation of vacancies in the common interaction zone intensifies the attractive force between the loops, resulting in coalescence even in conditions where both glide and climb are required to bring the process to completion.

The coalescence process is studied in the simulations presented in Fig. 5, where two elongated interstitial loops with nonoverlapping glide cylinders are placed at an offset distance of 10b from one another. While the loops here are simulated with Fe as the base material for direct comparison with experimental results of irradiated Fe in Ref. [29], we expect the simulated behavior to be qualitatively the same in other bcc metals. The relevant physical parameters that were used for Fe were $a_0 = 0.286$ nm, $H_f = 1.7$ eV, $E_m^0 = 0.68$ eV, $b = 0.25$ nm, $\Omega_a = 0.80b^3$, and $\Omega_{\text{rel}} = -0.2$. The offset separation d_v is along the "vertical" direction in the figure and is overcome by glide, while the glide cylinders are brought into contact by climb along the "horizontal" direction, d_h. We then let the loops evolve under no external applied stress, and we track d_v and d_h. The results are shown in Fig. 5(a), where both distances are seen to decrease monotonically to zero. The angle θ representing the ratio of the glide and climb distances [as $\theta = \tan^{-1}(d_h/d_v)$] is also included in the figure. The process is eminently elastic, as demonstrated by the good agreement between our time-dependent evolution and Kroupa's

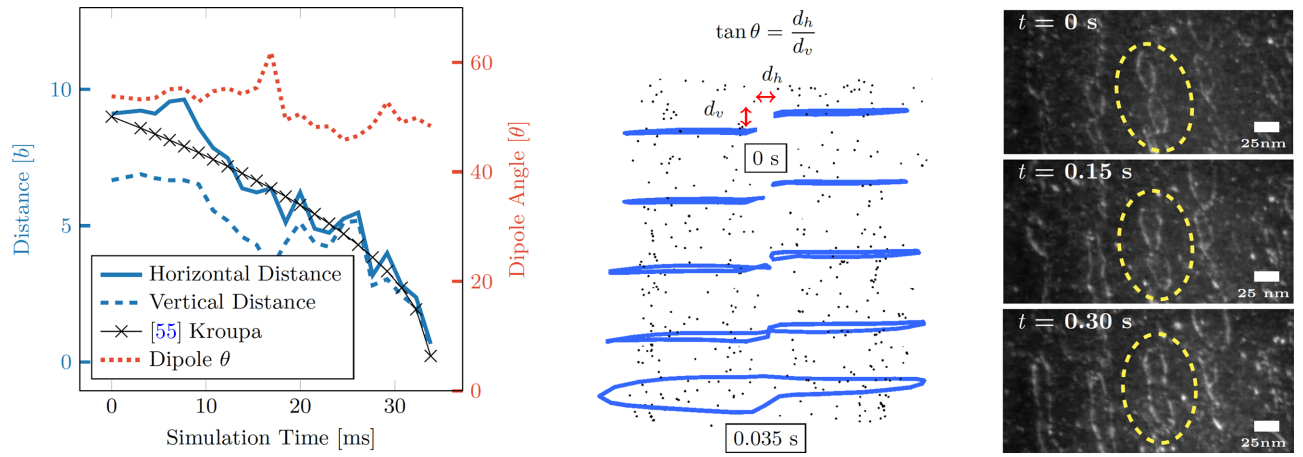

FIG. 5. (a) Horizontal (blue solid curve) and vertical separation (blue dashed curve) between an interstitial prismatic loop dipole and the corresponding dipole angle (dotted red curve, right axis) as a function of simulation time. The dipole angle remains relatively constant as the loops climb and glide towards one another and eventually annihilate the dipole. (b) Snapshots of the interstitial loop dipole shrinking and eventually coalescing under combined climb-glide mechanics. (c) Coalescence process of two irradiation loops in pure Fe at 300 °C (from Ref. [29], reproduced with permission). Scale bar: 25 nm equals approximately 100b in Fe.

expression to describe climb-mediated annihilation of two pure edge dislocations [55]:

$$\frac{1}{2}\left(\frac{h}{bK}\right)^2 \approx \frac{1}{2}\left(\frac{h_0}{bK}\right)^2 - \frac{2D_v c_j}{b^2 K}t, \tag{7}$$

where h is the dipole width (here equivalent to d_h), K is a temperature-dependent material parameter, c_j is the density of jogs on the dislocation, t is time, and h_0 is the initial climb offset at $t = 0$. As the figure shows, the offset angle remains practically constant during the coalescence process. Figure 5(b) shows several snapshots of the coalescence simulations. The loops expand via climb while also gliding towards one another to bridge the separation d_v. However, climb outpaces glide, and in the end a jog of magnitude $\approx d_v$ is left in the coalesced structure. The simulated process is remarkably similar to *in situ* transmission electron microscopy (TEM) observations of prismatic loop coalescence in irradiated Fe at 300 °C [29], as displayed in Fig. 5(c). While the origin of the loops differs, once formed, the kinetics of coalescence seen in the experiments matches what our simulations predict. This is a very encouraging sign that adds confidence to our models. Videos of the coalescence process observed with both *in situ* TEM and the computational method are provided in the Supplemental Material [37] as well. Additionally, we note that the loop configuration in Fig. 5(b) was constructed as an arbitrary dipole but allowed to evolve freely. Both the kinetics and final configuration may strongly depend on the type of multiloop metastable configuration that the dislocations adopt, but a detailed examination is beyond the scope of this Research Letter [34].

Summary. Our first finding of significance is the existence of a stress minimum around a prismatic loop that can create an elastic trap for point defects at an offset distance on the order of $2b$ to $5b$ from the actual loop segments. This trap is located outside the perimeter for vacancy loops (inside for self-interstitial loops). While a sizable kinetic barrier exists to access this minimum when approaching the loop from its habit plane, we find that vacancies take advantage of a "cone" of favorable (compressive) stress gradients to approach the loops and become trapped there. The significance of this is that for isolated loops, vacancies are not immediately absorbed by the dislocation segments, which is the common assumption to formulate osmotic forces that balance prismatic loops against climb. A more detailed investigation of the influence of vacancy cluster formation and inelastic interactions between the vacancies and dislocation cores is needed to capture the ultimate fate of these structures but is presently beyond the scope of this Research Letter.

Second, we find that in a coalescence process between two prismatic loops belonging to nonoverlapping glide cylinders, the stress traps belonging to each loop merge and intensify. This actually favors climb, as a relatively large concentration of vacancies is funneled to that region, creating extra chemical force for absorption. Coalescence is thus directly driven by elastic forces that bring the loops in line via glide, and indirectly through climb (chemical) forces that expand their glide cylinders until contact is established and coalescence takes place. We find a remarkable qualitative agreement with *in situ* TEM observations of similar processes in irradiated Fe. None of these effects can be effectively studied via direct atomistic simulations—as the configurational space and the relevant time scales are simply far too large to be explored rigorously—or with continuum methods because they fail to capture the fine details of the interactions between point defects and dislocation segments, including fluctuations.

Acknowledgments. C.M. and J.M. acknowledge support from the U.S. Department of Energy, Office of Fusion Energy Sciences, under Project No. DE-SC0019157. Lawrence Livermore National Laboratory is operated by Lawrence Livermore National Security, LLC, for the U.S. Department of Energy, under Contract No. DE-AC52-07NA27344 (Release No. LLNL-JRNL-810758).

[1] H. Kimura, D. Kuhlmann-Wilsdorf, and R. Maddin, Appl. Phys. Lett. **3**, 4 (1963).
[2] P. Humble, M. Loretto, and L. Clarebrough, Philos. Mag. **15**, 297 (1967).
[3] S. Kojima, Y. Satoh, H. Taoka, I. Ishida, T. Yoshiie, and M. Kiritani, Philos. Mag. A **59**, 519 (1989).
[4] Y. Matsukawa, Y. Osetsky, R. Stoller, and S. Zinkle, Philos. Mag. **88**, 581 (2008).
[5] K. Westmacott, R. Barnes, D. Hull, and R. Smallman, Philos. Mag. **6**, 929 (1961).
[6] P. Hirsch, J. Silcox, R. Smallman, and K. Westmacott, Philos. Mag. **3**, 897 (1958).
[7] R. Smallman and K. Westmacott, J. Appl. Phys. **30**, 603 (1959).
[8] S. Amelinckx and P. Delavignette, Phys. Rev. Lett. **5**, 50 (1960).
[9] M. Makin and S. Manthorpe, Philos. Mag. **8**, 1725 (1963).
[10] J. Meakin, A. Lawley, and R. Koo, Appl. Phys. Lett. **5**, 133 (1964).
[11] Z. Gierak, J. Moroń, and A. Lehr, Phys. Status Solidi (a) **77**, 775 (1983).
[12] S. Yoshida, N. Nagata, and Y. Ohba, Trans. Jpn. Inst. Met. **5**, 155 (1964).
[13] K. Yamakawa and Y. Shimomura, J. Nucl. Mater. **271–272**, 41 (1999).
[14] M. Wen, N. M. Ghoniem, and B. N. Singh, Philos. Mag. **85**, 2561 (2005).
[15] S. Dudarev, K. Arakawa, X. Yi, Z. Yao, M. Jenkins, M. Gilbert, and P. Derlet, J. Nucl. Mater. **455**, 16 (2014).
[16] O. El-Atwani, E. Aydogan, E. Esquivel, M. Efe, Y. Wang, and S. Maloy, Acta Mater. **147**, 277 (2018).
[17] L. Bragg, Nature (London) **149**, 511 (1942).
[18] D. Kuhlmann-Wilsdorf, Metall. Trans. A **16**, 2091 (1985).
[19] A. D. Rollett and U. Kocks, Solid State Phenom. **35–36**, 1 (1993).
[20] P. A. Beck, Adv. Phys. **3**, 245 (1954).
[21] A. Van den Beukel, Acta Metall. **11**, 97 (1963).
[22] A. Belyakov, K. Tsuzaki, Y. Kimura, and Y. Mishima, J. Mater. Res. **22**, 3042 (2007).
[23] I. Rovelli, S. L. Dudarev, and A. P. Sutton, Phys. Rev. E **98**, 043002 (2018).

[24] A. Chauhan, Q. Yuan, C. Dethloff, E. Gaganidze, and J. Aktaa, J. Nucl. Mater. **548**, 152863 (2021).
[25] J. Silcox and M. Whelan, Philos. Mag. **5**, 1 (1960).
[26] C. Johnson, Philos. Mag. **5**, 1255 (1960).
[27] J. Turnbull, Philos. Mag. **21**, 83 (1970).
[28] M. Kiritani, N. Yoshida, H. Takata, and Y. Maehara, J. Phys. Soc. Jpn. **38**, 1677 (1975).
[29] M. Hernández-Mayoral, Z. Yao, M. Jenkins, and M. Kirk, Philos. Mag. **88**, 2881 (2008).
[30] K. Arakawa, T. Amino, and H. Mori, Acta Mater. **59**, 141 (2011).
[31] B. Bakó, E. Clouet, L. M. Dupuy, and M. Blétry, Philos. Mag. **91**, 3173 (2011).
[32] D. Mordehai and G. Martin, Phys. Rev. B **84**, 014115 (2011).
[33] X. Niu, Y. Gu, and Y. Xiang, Int. J. Plast. **120**, 262 (2019).
[34] Y. Li, M. Boleininger, C. Robertson, L. Dupuy, and S. L. Dudarev, Phys. Rev. Mater. **3**, 073805 (2019).
[35] F. Liu, A. C. Cocks, S. P. Gill, and E. Tarleton, Modell. Simul. Mater. Sci. Eng. **28**, 055012 (2020).
[36] C. McElfresh, Y. Cui, S. L. Dudarev, G. Po, and J. Marian, Int. J. Plast. **136**, 102848 (2021).
[37] See Supplemental Material at http://link.aps.org/supplemental/10.1103/PhysRevMaterials.6.L100601 for a demonstration of how the exact solution of Eq. (1), i.e., with spatially dependent $\boldsymbol{u}$, can be satisfactorily approximated by Eq. (2) within the timescales of vacancy diffusion; figures providing evidence of vacancy clustering behavior on the inside of interstitial prismatic loops; and videos of the coalescence process observed with both *in situ* TEM and the computational method.
[38] C. McElfresh, N. Bertin, S. Aubry, and J. Marian, Comput. Mater. Sci. **209**, 111332 (2022).
[39] J. Friedbl and M. Yoshida, Philos. Mag. **31**, 229 (1975).
[40] E. Clouet, Acta Mater. **54**, 3543 (2006).
[41] M. A. Puigvi, N. de Diego, A. Serra, Y. N. Osetsky, and D. J. Bacon, Philos. Mag. **87**, 3501 (2007).
[42] M. Kabir, T. T. Lau, D. Rodney, S. Yip, and K. J. Van Vliet, Phys. Rev. Lett. **105**, 095501 (2010).
[43] P.-W. Ma and S. L. Dudarev, Phys. Rev. Mater. **3**, 063601 (2019).
[44] P.-W. Ma and S. L. Dudarev, Phys. Rev. Mater. **3**, 013605 (2019).
[45] V. Bulatov, W. Cai, J. Fier, M. Hiratani, G. Hommes, T. Pierce, M. Tang, M. Rhee, K. Yates, and T. Arsenlis, in *SC'04: Proceedings of the 2004 ACM/IEEE Conference on Supercomputing* (IEEE, Piscataway, NJ, 2004), p. 19.
[46] Z. Wang, N. Ghoniem, S. Swaminarayan, and R. LeSar, J. Comput. Phys. **219**, 608 (2006).
[47] W. Cai, V. V. Bulatov, T. G. Pierce, M. Hiratani, M. Rhee, M. Bartelt, and M. Tang, in *IUTAM Symposium on Mesoscopic Dynamics of Fracture Process and Materials Strength* (Springer, New York, 2004), pp. 1–11.
[48] E. Martínez, J. Marian, M. H. Kalos, and J. M. Perlado, J. Comput. Phys. **227**, 3804 (2008).
[49] E. Martínez, P. R. Monasterio, and J. Marian, J. Comput. Phys. **230**, 1359 (2011).
[50] In bcc metals, prismatic loops adopt a hexagonal shape whose edges are oriented along ⟨112⟩ directions [56].
[51] W. Cai, A. Arsenlis, C. R. Weinberger, and V. V. Bulatov, J. Mech. Phys. Solids **54**, 561 (2006).
[52] A. Arsenlis, W. Cai, M. Tang, M. Rhee, T. Oppelstrup, G. Hommes, T. G. Pierce, and V. V. Bulatov, Modell. Simul. Mater. Sci. Eng. **15**, 553 (2007).
[53] E. Martinez, J. Marian, A. Arsenlis, M. Victoria, and J. M. Perlado, J. Mech. Phys. Solids **56**, 869 (2008).
[54] Note2, the *glide cylinder* or *glide prism* is the quadric surface created by extending each of the loop's edges (or the entire perimeter in the case of a circular loop) to infinity along the Burgers vector's direction.
[55] F. Kroupa, Czech. J. Phys. B **17**, 220 (1967).
[56] J. Marian, B. Wirth, R. Schäublin, J. Perlado, and T. D. de la Rubia, J. Nucl. Mater. **307–311**, 871 (2002).